ACS NANO

www.acsnano.org

ARTICLE

Molecular Sieving Across Centimeter-Scale Single-Layer Nanoporous Graphene Membranes

Michael S. H. Boutilier,[†] Doojoon Jang,[†] Juan-Carlos Idrobo,[‡] Piran R. Kidambi,[†] Nicolas G. Hadjiconstantinou,*[,†] and Rohit Karnik*[,†]

[†]Department of Mechanical Engineering, Massachusetts Institute of Technology, 77 Massachusetts Avenue, Cambridge, Massachusetts 02139, United States

[‡]Center for Nanophase Materials Sciences, Oak Ridge National Laboratory, Oak Ridge, Tennessee 37831, United States

Supporting Information

ABSTRACT: **Molecular sieving across atomically thin nanoporous graphene is predicted to enable superior gas separation performance compared to conventional membranes. Although molecular sieving has been demonstrated across a few pores in microscale graphene membranes, leakage through nonselective defects presents a major challenge toward realizing selective membranes with high densities of pores over macroscopic areas. Guided by multiscale gas transport modeling of nanoporous graphene membranes, we designed the porous support beneath the graphene to isolate small defects and minimize leakage through larger defects. Ion bombardment followed by oxygen plasma etching was used to produce subnanometer pores in graphene at a density of ~10^{11} cm^{-2}. Gas permeance measurements demonstrate selectivity that exceeds the Knudsen effusion ratio and scales with the kinetic diameter of the gas molecules, providing evidence of molecular sieving across centimeter-scale nanoporous graphene. The extracted nanoporous graphene performance is comparable to or exceeds the Robeson limit for polymeric gas separation membranes, confirming the potential of nanoporous graphene membranes for gas separations.**

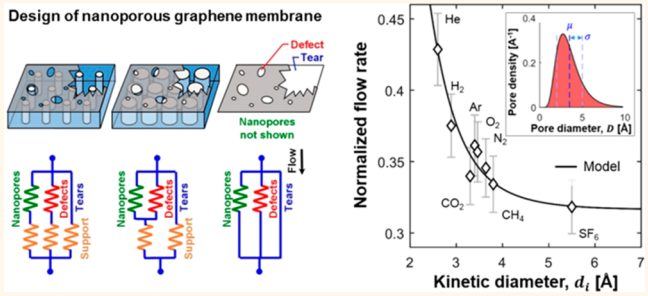

KEYWORDS: *gas separation, graphene, membranes, two-dimensional materials, nanofluidics, atomically thin, leakage*

Industrial gas separations, such as natural gas sweetening, hydrogen separation from syngas, and carbon capture, can be accomplished by sorption, distillation, or membrane separations.[1−4] Membrane processes are generally attractive because of their modular, compact nature, and lower energy requirements, but can be limited by the inherent trade-off between the flow rate and selectivity of conventional solution-diffusion membranes (Robeson performance limit).[1,5] This restriction necessitates very large areas or compromising on selectivity to achieve the required throughput.

Nanoporous graphene membranes have the potential to address these limitations by exceeding the permeance and selectivity limits of existing gas separation membranes.[6] This is made possible by the atomic thickness of graphene, leading to low resistance to permeate flow and allowing the membrane to support subnanometer pores that can separate molecules by size-exclusion (molecular sieving). Numerous classical molecular dynamics and *ab initio* simulations have predicted that graphene has the potential to provide order of magnitude performance improvements over the Robeson performance limit of polymer membranes (*e.g.*, refs 7−9).

The feasibility of gas separation using graphene membranes was demonstrated by Koenig *et al.*[10] on a microscale area of mechanically exfoliated graphene made porous by UV-ozone etching. They demonstrated molecular sieving with a measured H_2/CH_4 selectivity exceeding 15,000. The potentially high gas permeance of graphene was later demonstrated with helium-ion beam milled graphene on silicon supports by Celebi *et al.*[11] Although the smallest pores they produced (~7.6 nm diameter compared to <0.6 nm kinetic diameters of gas molecules)[12] were too large for molecular sieving, these pores were sufficiently smaller than the mean free path of gas molecules to operate in a Knudsen effusion regime, where modest selectivities result from differences in molecule mass, and hence, in average molecule speed. Furthermore, with ~10^6

Received: February 21, 2017
Accepted: June 2, 2017
Published: June 13, 2017

DOI: 10.1021/acsnano.7b01231
ACS Nano 2017, 11, 5726−5736

pores and 4% porosity, they achieved orders of magnitude higher permeance than that given by the Robeson limit for the same selectivity.

Industrial gas separation membranes typically require areas of thousands of square meters.[2] However, macroscopic areas of graphene contain defects in the nanometer size range[13] that can create nonselective leakage pathways for gas molecules.[13,14] Larger defects, up to micron-scale, can also be formed during membrane fabrication by transfer of graphene grown by chemical vapor deposition (CVD) onto porous support substrates, producing additional leakage pathways. These defects can render the membrane ineffective. Furthermore, whereas single pores in the subnanometer size range required for molecular sieving can be produced,[10] and arrays of larger pores can be patterned,[11] scaling up of nanoporous graphene membranes requires methods to create a high density of selective subnanometer pores over macroscopic areas. Production of subnanometer pores at a density of $\sim 10^{12}$–10^{13} cm^{-2} over centimeter-scale graphene by ion bombardment, followed by potassium permanganate etching has been reported by O'Hern *et al.*[13] Surwade *et al.*[15] demonstrated that oxygen plasma etching of graphene can create ~1 nm pores suitable for high flux water pervaporation.[16] Pores created by these methods exhibit a distribution of sizes, which is detrimental to gas selectivity, particularly for separations of gases with similar molecule size. The extent to which large-area nanoporous graphene membranes with subnanometer pores created by existing methods will exhibit selectivity to gases is therefore unclear.

In summary, mitigation of leakage through defects and creation of a high density of selective subnanometer pores are the two most immediate challenges toward practical, large-scale, high-performance, molecular-sieving-based graphene membranes. Our study aims to address these challenges by focusing on the design, fabrication, and performance evaluation of centimeter-scale nanoporous graphene membranes.

RESULTS AND DISCUSSION

Creating a high density of selective nanopores is not sufficient to achieve selective gas transport through macroscopic areas of graphene because nonselective leakage through defects can easily exceed flow through selective pores by several orders of magnitude.[14] Minimizing leakage flow is therefore an essential aspect of membrane design. Although leakage mitigation is possible by constructing membranes from two or more layers of graphene, where additional layers cover defects in the first layer (Supporting Information Figure S8a),[11,14,17] this approach can make selective pore creation more difficult. Similarly, although methods are available to seal defects in graphene membranes,[18,19] our studies (Figure S8c) show that further development is needed for these techniques to function adequately on gas separation membranes. In this work, we adopted a simpler approach to leakage mitigation: designing a porous support layer for the nanoporous graphene that can reduce leakage.

Design of Optimal Support Layer. Although defects in macroscopic areas of graphene have a range of sizes from subnanometer to micron-scale, for modeling purposes, we separate defects into large tears or small intrinsic defects,[13,14] where "large" and "small" are in comparison to the size of the support layer pores. Tears can originate from handling and transfer of graphene during membrane fabrication and are characterized by the coverage, γ, defined as the fraction of support pores covered with tear-free graphene. Intrinsic defects occur primarily during graphene synthesis and are characterized by the intrinsic porosity, η. Tears present a significantly lower resistance to gas flow than selective nanopores in graphene, creating a short circuit for gas transport around the nanoporous graphene (Figure 1d). By choosing a support layer consisting of parallel pores that provide isolated transport pathways, leakage flow through tears can be confined to the support layer pores

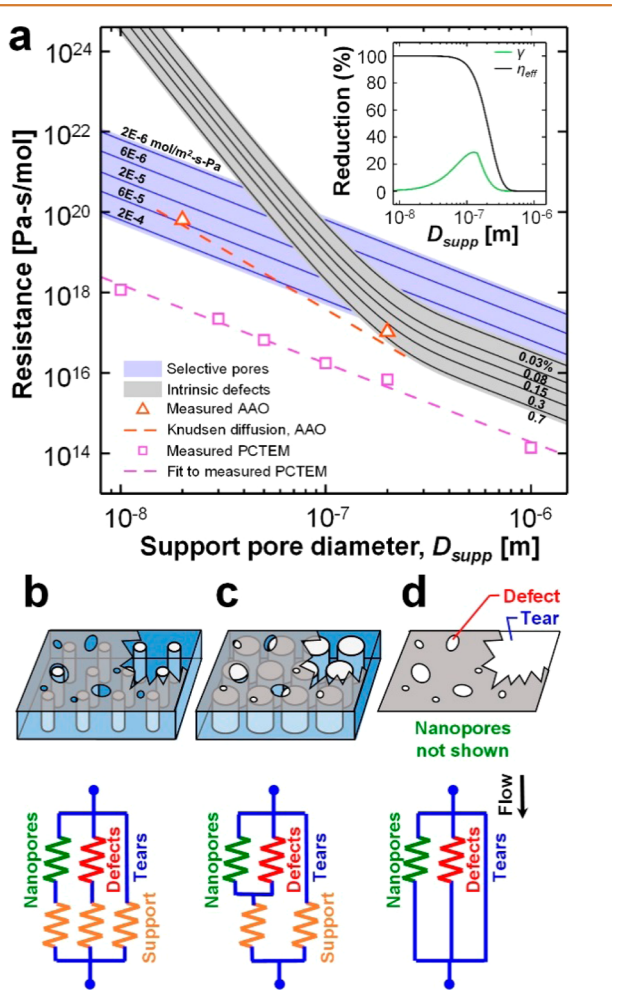

Figure 1. Membrane design. (a) Helium gas flow resistance of support pore and graphene over a support pore as a function of support pore diameter. The resistance of graphene (over a support pore) due to intrinsic defects and selective pores is shown for different values of intrinsic porosity and permeance due to selective pores, respectively. This intrinsic defect resistance includes only those defects with higher resistance than the AAO pores. Measured AAO pore resistance is compared to Knudsen diffusion predictions. Inset further illustrates the effect of intrinsic defect isolation, by plotting the percentage change in graphene coverage (γ) and effective defect porosity (η_{eff}) as support pore size is reduced. Inset is for 0.3% intrinsic porosity and 70% coverage in the large support pore limit. Further details on how these resistances were estimated are provided in the Supporting Information. (b–d) Careful selection of the support pore diameter and flow resistance can limit leakage flow through large tears and isolate smaller defects. (b) By reducing support pore size, defects are isolated to a small fraction of the support pores. (c) Leakage is reduced by adding an effective resistance in series. (d) Graphene section with no support. Nanopores, not shown here, are assumed to be uniformly distributed.

DOI: 10.1021/acsnano.7b01231
ACS Nano 2017, 11, 5726–5736

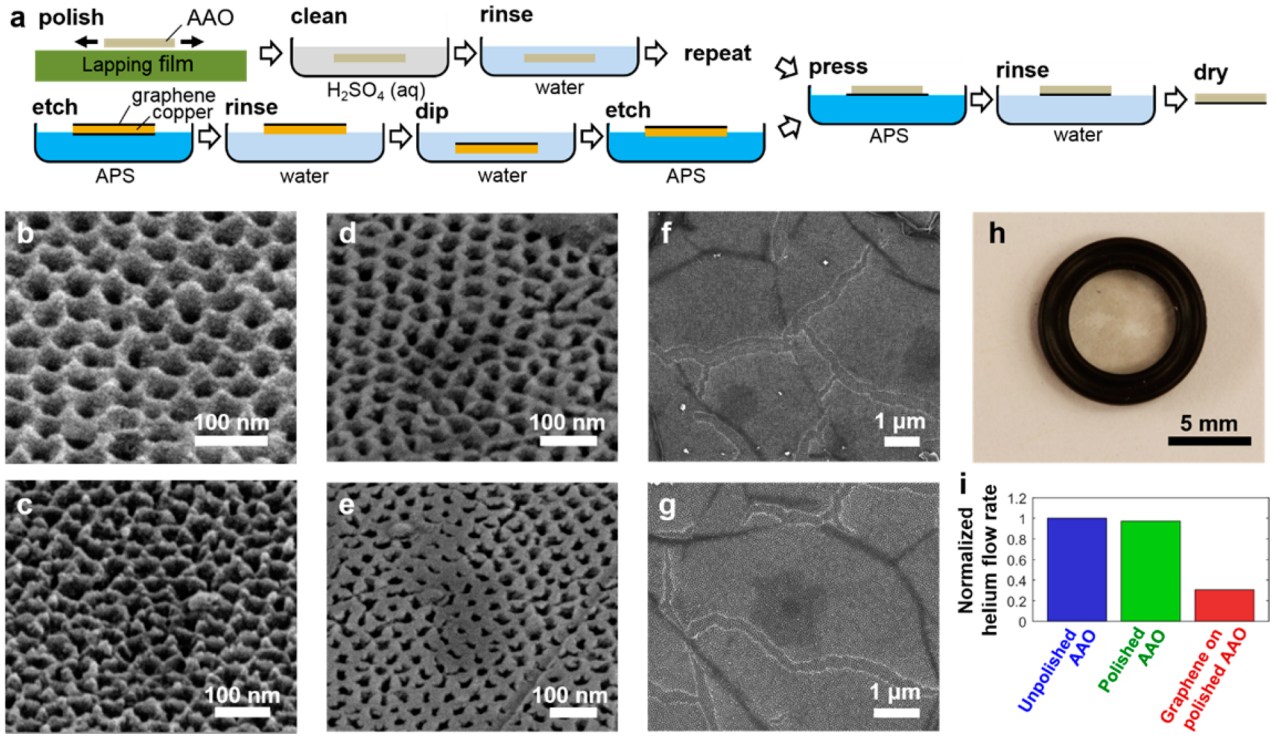

Figure 2. Membrane fabrication. (a) Graphene is transferred to polished 20 nm pore diameter AAO membranes by a direct pressing procedure. (b–g) SEM images of unpolished AAO taken at an angle of 52° from vertical (b,c), polished AAO taken at an angle of 52° from vertical (d,e), and graphene on a polished AAO taken at a vertical angle (f,g). (h) Photograph of graphene on a polished AAO membrane, with O-ring attached for gas measurements. (i) Helium flow rate through an AAO support before polishing, after polishing, and after graphene transfer.

immediately below the tears (Figure 1b,c). Furthermore, by selecting a support pore resistance that is similar to the gas flow resistance due to selective pores in graphene, nonselective leakage flow through tears is limited to a value similar to that through selective pores in graphene. In doing so, it should be possible to produce a selective graphene membrane despite the presence of tears. Note that there is an optimal value of the support resistance where membrane selectivity is maximized; too low a resistance will result in high leakage flow, whereas too high a resistance will cause the nanoporous graphene to have a negligible effect on membrane permeance. In other words, choosing a support layer with its resistance matched to that of selective pores in nanoporous graphene will mitigate leakage but largely retain the permeance achievable by nanoporous graphene.[14]

In order to select a matched support membrane, a reliable estimate of the selective-pore permeance in graphene is needed. Here, permeance is defined as the flow rate per unit area per unit pressure differential and is related to resistance *via* the relation: resistance = (permeance × area)$^{-1}$. Based on reported single pore measurements,[20] simulations,[7−9,21] and created pore densities,[15,18] we estimated the achievable range of permeance to be approximately 2×10^{-6} to 2×10^{-4} mol/m^2·s·Pa. The gas flow resistance of an area of nanoporous graphene over a support pore of diameter D_{supp} due to selective pores is plotted in Figure 1a. The resistance is proportional to D_{supp}^{-2}, since the number of selective pores over the support pore is proportional to the graphene area. In the same figure, this resistance is compared to that of the pores of two types of commercially available support membranes with the desirable isolated pore structure: polycarbonate track-etched membranes (PCTEMs, Sterlitech) and anodic aluminum oxide membranes (AAO, InRedox) with constant pore diameter throughout the thickness. The gas flow resistance of the PCTEM pores is orders of magnitude below the selective pore resistance range; leakage will therefore dominate transport for this choice of support (see ref 14 for a discussion of these issues in more detail). On the other hand, AAO membranes can be selected with resistance in the desired range.

Intrinsic Defect Isolation. In addition to tears, intrinsic defects also form nonselective leakage pathways through graphene. Intrinsic defects are sufficiently small (subnanometer to few-nanometer) that their resistance is high compared to the support pore, but can still impair membrane selectivity if their permeance is comparable to or higher than that due to the selective pores, especially given their typically large number density in CVD graphene.[14] The estimated graphene resistance due to intrinsic defects is plotted in Figure 1a for intrinsic porosities of 0.03−0.7%, typical of previously reported CVD graphene[14] (Supporting Information Section I and Figure S1a). As we discuss below, it is possible to reduce leakage through intrinsic defects by careful support membrane design. Given a mean spacing between defects, the larger the support-membrane pores (Figure 1c), the higher the probability that they will be covered by graphene with one or more intrinsic defects, undermining the contribution of each support pore and thus limiting the overall selectivity of the membrane. By instead choosing a support pore diameter that is small compared to the defect spacing (estimated to be in the range of 100 nm),[14] defects can be isolated to a small fraction of the support pores, limiting the extent of their influence and leaving a large number

DOI: 10.1021/acsnano.7b01231
ACS Nano 2017, 11, 5726−5736

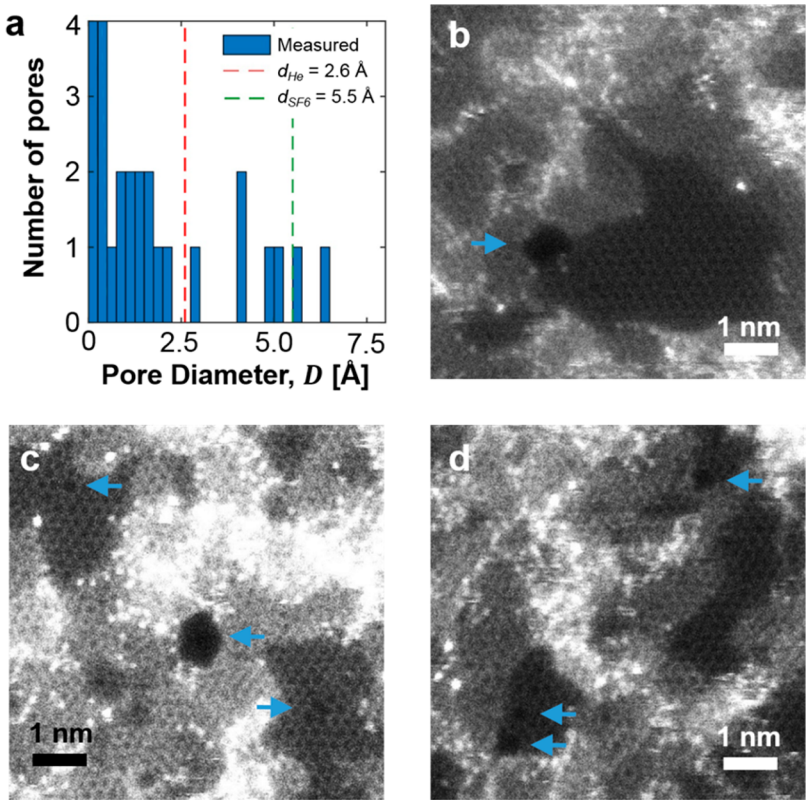

Figure 3. Selective pore characterization. (a) Pore size distribution estimated from STEM images of graphene on a TEM grid bombarded with gallium ions at 5 × 10^{12} ions/cm^2, 52° incidence, and 1 kV accelerating voltage and plasma-etched for 30 s. The plotted pore diameter is that of a circle of the same area as the imaged pore, corrected for the van der Waals diameter of carbon, as described in Supporting Information Section VII. The total imaged area was 6400 nm^2. (b–d) Example STEM images of pores created in graphene. The hexagonal graphene lattice is visible in sections of each image. Note that many areas are covered in bright contamination. Pores are visible as dark gaps in the graphene lattice and are indicated by blue arrows. Tears and intrinsic defects have a much larger spacing than the field of view and are not present in these images.

of support pores covered by pristine graphene that can have very high selectivity (once selective pores are created).[14]

Defect isolation can be quantitatively illustrated by the steep rise in intrinsic defect resistance as the support pore diameter is reduced below approximately 100 nm (Figure 1a). This behavior was estimated with the model described in the Supporting Information Section I and uses the intrinsic defect size distribution in CVD graphene extracted from high-resolution images (Figure S1b).[13] This rise occurs because, as the support pore size is reduced, flow through larger intrinsic defects is limited by the increasing resistance of the underlying support pore (Figures 1a and S1b,c). This effect can be further quantified by defining an effective defect porosity (η_{eff}) based on small defects; defects are considered small if their resistance is greater than that of the support pore. When the support pore size is large, almost all defects present a resistance that is smaller than that of the support pore (Figure 1a, inset). However, as the support pore size decreases, the resistance of the support pore becomes larger than that of some defects, which then effectively contribute to a slightly reduced graphene coverage, γ (since the total area occupied by defects is typically <1%). As a result, according to this model, for small support pore diameters, the reduction in effective defect porosity is significant, whereas the change in graphene coverage is negligible (Figure 1a, inset). The latter conclusion follows by noting that, although large defects act as tears (resistance smaller than the support pore resistance), the spatial extent of their influence decreases quadratically with the support pore diameter.

Based on the above criteria of defect isolation and resistance matching, we chose 50 μm-thick AAO membranes with isolated, 20 nm diameter pores of uniform cross section throughout their thickness as the support layer (InRedox, Figure S4f). The support pore resistance measured for this AAO membrane (6.4 × 10^{19} Pa·s/mol) is well matched (Figure 1a) to the resistance of defect-free nanoporous graphene (*i.e.*, to the resistance of selective pores in graphene over an area 20 nm in diameter), which equals 5.3 × 10^{19} Pa·s/mol for nanoporous graphene with a permeance of 6 × 10^{-5} mol/m^2·s·Pa. The support pore diameter of 20 nm should also provide good defect isolation, since it is smaller than the average spacing between intrinsic defects, estimated to be ~100 nm.[13,14] The estimated resistance to flow through intrinsic defects for this support (5.1 × 10^{22} Pa·s/mol) is therefore significantly higher than that of selective pores in graphene and of the support pore. Graphene leakage is mitigated with this choice of AAO pore diameter, but would not be for larger AAO pore sizes (Figure 1a). Although AAO membranes with smaller pore diameters would also be acceptable, those are only commercially available in smaller thicknesses that lead to reduced support resistance. The 20 nm AAO membrane is therefore the optimal candidate for the support layer from among the commercially available membranes considered here.

DOI: 10.1021/acsnano.7b01231
ACS Nano 2017, 11, 5726–5736

Membrane Fabrication and Characterization. Fabrication of the nanoporous graphene membranes requires transfer of graphene grown on copper by CVD to the AAO support. One of the challenges in transferring graphene onto the AAO support is that the latter has a rough surface (Figure 2b,c). This could result in a lower success rate of graphene transfer, torn graphene, or gaps between the graphene and AAO surface, leading to lateral gas transport through these gaps that prevents isolation of leakage pathways. To mitigate these issues, the AAO membranes were mechanically polished (Figures 2a and S2), creating a smooth surface (Figure 2d,e) without blocking gas flow through the AAO pores (Figure 2i). The copper foil on which the CVD graphene is grown was chemically removed, leaving graphene floating on the etchant (Figures 2a and S2). The polished AAO surface was then pressed into the floating graphene from above, and the assembly was rinsed before air drying. This graphene transfer method is polymer-free and therefore minimizes the possibility of surface contamination. A 10 mm diameter graphene membrane fabricated in this way is shown in Figure 2h. SEM images of the surface (Figure 2f,g) show isolated dark streaks of highly abraded material formed during polishing as well as lighter stripes that appear to not have graphene, possibly forming in areas where there were wrinkles in the graphene on copper.

Various methods were considered for selective pore creation. Selective pore densities reported in bilayer graphene by UV ozone etching ($\sim 10^7$ pores/cm^2)[20] are lower than what has been achieved by other methods. Electron beam irradiation[22] is difficult to scale to centimeter areas, while ion beam milling[11] produces pores too large for gas molecule sieving. The AAO membranes are incompatible with the acidic potassium permanganate etchant previously used for creating a high density of subnanometer pores.[18,19] Oxygen plasma etching[15] was chosen for selective pore creation because it can produce small pores with high density ($\sim 10^{12}$ pores/cm^2) over centimeter-scale areas. The graphene membranes were bombarded with gallium ions at densities of $2-6 \times 10^{13}$ ions/cm^2 prior to plasma exposure in an effort to increase the pore density.

Aberration-corrected scanning transmission electron microscopy (STEM) of a graphene sample on a TEM grid demonstrated that ion bombardment followed by oxygen plasma etching can produce subnanometer pores in graphene (Figure 3). Although 85% of the 48 pores imaged on this sample have pore diameters smaller than the kinetic diameter of helium (2.6 Å),[12] the density of pores larger than this size is approximately 1.1×10^{11} pores/cm^2. This density of helium-permeable pores should be sufficient for the nanoporous graphene resistance to be in the range required for the membrane to function as designed (Figure 1a).

Helium (He) and sulfur hexafluoride (SF_6) were chosen for initial tests of selective gas transport because they have relatively simple molecular structures and significantly different kinetic diameters. For the measured pore size distribution in Figure 3a, five of the seven pores that are larger than helium (2.6 Å) are smaller than the kinetic diameter of sulfur hexafluoride (5.5 Å).[12] Pores that are slightly larger than sulfur hexafluoride should still exhibit some selectivity because of the greater steric hindrance of the larger gas molecule passing through such pores.

Selective Gas Permeance. To screen for pore creation parameters that would result in selective transport, gas flow rates were measured for four ion-bombarded graphene membranes (Table S1) between short intervals of plasma exposure (Figure 4). Permeance increased with etch time as the membranes became more porous (Figure 4a). By 300 s of plasma exposure, the graphene was largely removed, and the flow rate returned to near that of a polished AAO support without graphene (Figures 4 and S5; three membranes broke before graphene was completely etched). The He/SF_6 selectivity peaked at shorter plasma etch times, before falling to that of the AAO support without graphene at long times. The maximum measured selectivity of ~8.4 exceeds the Knudsen selectivity of ~6.0. Since the Knudsen selectivity is the maximum attainable by differences in molecular mass and in the absence of adsorption (which is negligible for He),

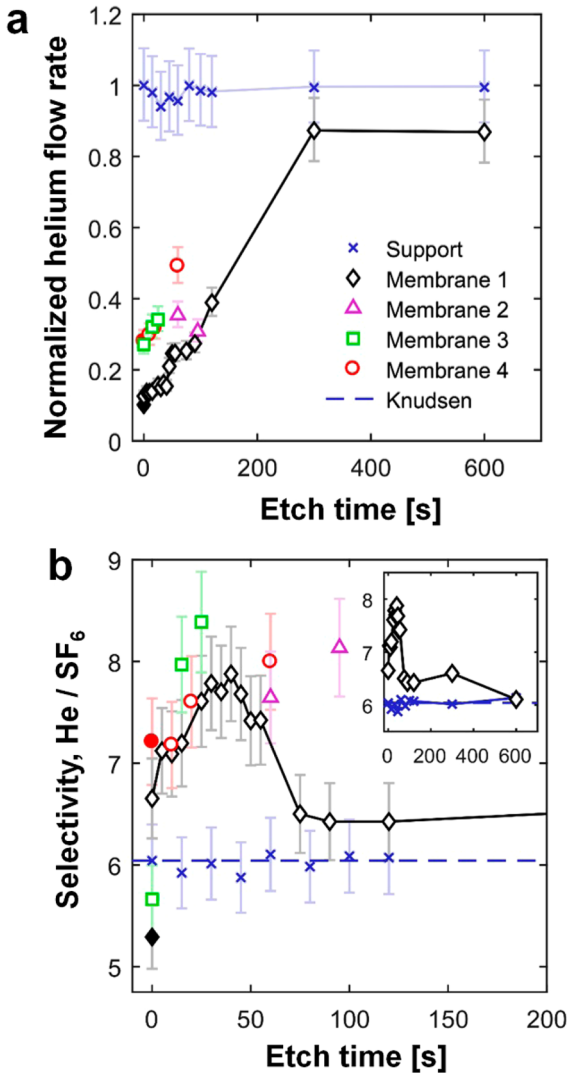

Figure 4. Effect of plasma etch time on gas permeance and selectivity. (a) Helium flow rates, normalized by that through the AAO membrane before graphene transfer. (b) He/SF_6 flow rate ratio. Measurements are plotted for a bare support membrane and four graphene membranes. Membranes 1−3 were bombarded at 2×10^{13} ions/cm^2, whereas membrane 4 was bombarded at 6×10^{13} ions/cm^2. Solid black and red markers are for graphene membranes 1 and 4, respectively, prior to ion bombardment. Further control measurements are presented in Figure S4. Uncertainty estimates are described in Supporting Information Section VIII and Table S3. Permeance data are listed in Table S4.

DOI: 10.1021/acsnano.7b01231
ACS Nano 2017, 11, 5726−5736

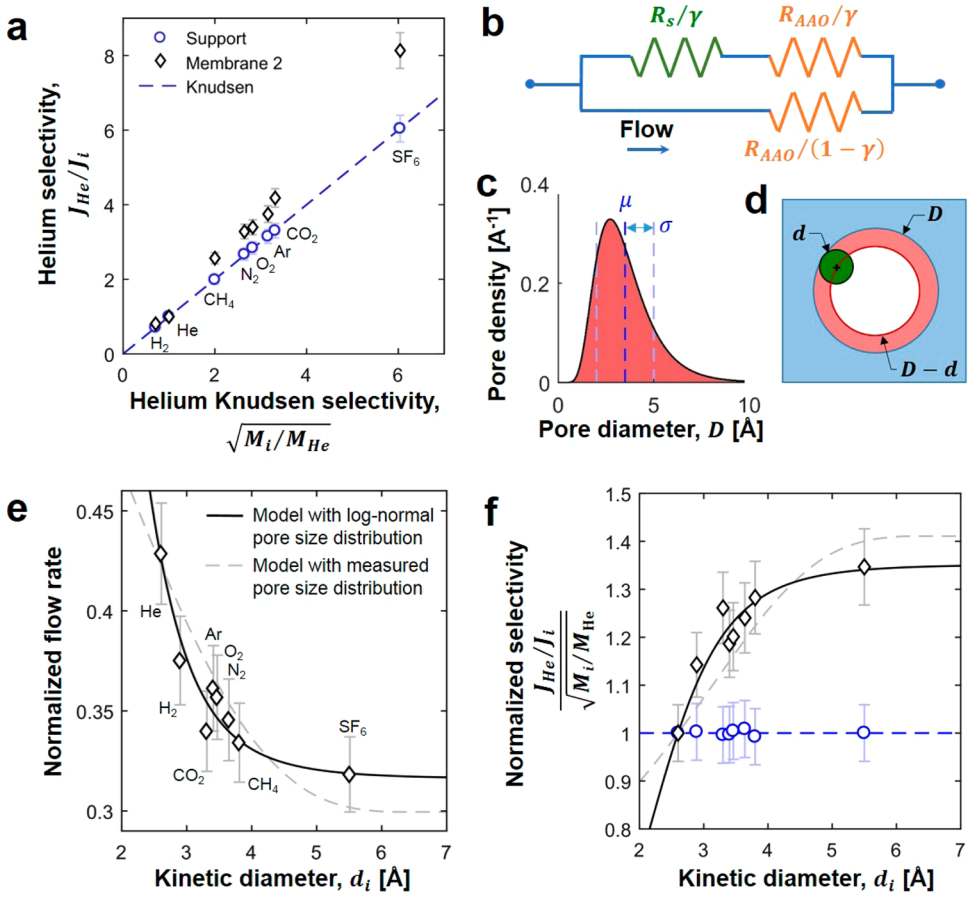

Figure 5. Dependence of permeance on molecule diameter. (a) Ratio of helium flow rate to that of other gases, plotted against the corresponding Knudsen selectivity. (b-d) Membrane permeance model. The equivalent resistance model (b), accounts for areas with graphene, which has a resistance due to selective pores of R_s and covers a fraction γ of the membrane, defects, where there is no graphene, and the resistance of the support pores, R_{AAO}. The model is applied using two different selective pore size distributions: the measured distribution in Figure 3a and a generic log-normal distribution. The log-normal pore size distribution (c) is specified by a mean (μ) and standard deviation (σ). The effective pore size (d) available for transport through a pore of diameter D and for a gas with molecule kinetic diameter d is approximated as $D - d$. (e) Gas flow rates, normalized by the flow rate of that gas through the AAO before graphene transfer, compared to the fitted models. (f) Flow rate ratio of helium to other gases, normalized by the corresponding Knudsen effusion value and compared to the models. The data plotted are for membrane 2, bombarded at 2×10^{13} ions/cm^2, after 95 s oxygen plasma exposure. The fitting parameters with a log-normal pore size distribution are $\mu = 0.0273$ Å, $\sigma = 0.0303$ Å, $\gamma = 0.684$, $\rho_s = 2.6 \times 10^{12}$ cm^{-2}, and with the measured distribution are $\gamma = 0.700$ and $\rho_s = 2.5 \times 10^{11}$ cm^{-2}. Permeance data for panels e,f are listed in Table S5.

exceeding this limit is evidence of molecular-sieving-based selective gas transport through centimeter-scale areas of graphene. The variation between results for membranes 1−3, which underwent the same pore creation treatment, is attributed to variability in graphene quality and an inability to reproduce exactly the same pore creation process due to frequent changes in the condition and configuration of the shared ion beam and plasma chamber.

The relatively large difference in kinetic diameters makes He/SF_6 separation a convenient choice for initial tests because it enhances measurement sensitivity to selective transport. After settling on pore creation conditions, gas permeance was measured on one membrane for several gases, covering a range of kinetic diameters and molecular masses (Figures 5 and S6 and Table S2). We report selectivities of helium relative to all other gases, to facilitate comparison to the Knudsen effusion selectivity. We find that selectivity increases with the difference in molecular mass (Figure 5a), reflecting the contribution of differences in molecule speeds to the permeance. Normalizing the selectivity by the corresponding Knudsen effusion selectivity (Figure 5f) removes this contribution. We find that, for all the gases measured, this normalized selectivity is correlated with kinetic diameter (Figures 5f and S6), providing further evidence of molecular-sieving-based selective gas transport.

Numerous computational studies have identified a contribution of adsorbed molecule diffusion on graphene to gas transport through graphene nanopores.[23−27] These simulations suggest that, with the exception of CO_2, the permeance enhancement resulting from surface diffusion increases with molecule size for the gases measured here. Consequently, the surface diffusion mechanism counteracts the selectivity enhancement afforded by near ballistic transport through size-selective nanopores. Adsorbed molecule diffusion could therefore not provide the measured selectivity above the Knudsen limit and, if occurring, is of secondary importance to gas transport through these membranes.

Permeance Modeling. A permeance model was developed to further the understanding of gas transport through these graphene membranes. It is based on an equivalent gas flow

DOI: 10.1021/acsnano.7b01231
ACS Nano 2017, 11, 5726−5736

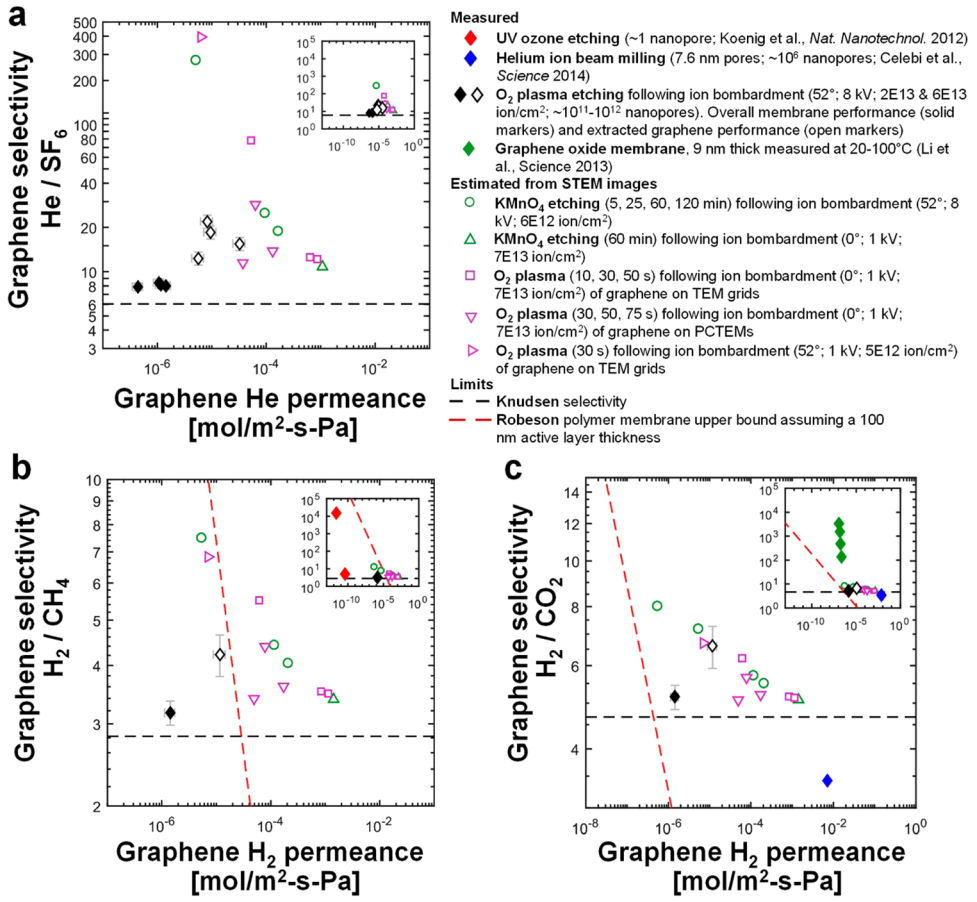

Figure 6. Graphene membrane performance. Overall membrane performance and extracted nanoporous graphene performance, compared to results from the literature and estimated performance from measured pore size distributions as described in the Supporting Information. (a) He/SF_6, (b) H_2/CH_4, and (c) H_2/CO_2. Graphene oxide data are for 9 nm-thick membranes by Li *et al.*,[30] and Robeson polymer membrane upper bounds are from Robeson[5] and assume a 100 nm-thick selective layer. Permeance data are listed in Tables S5 and S6. Membrane performance plots for other gas pairs are provided in Figure S10.

resistance model (Figure 5b) in which gas molecules can either pass through selective pores or tears in graphene. Tear-free graphene covers a fraction, γ, of the AAO pores. Gas passing through tears experiences only the resistance of the support pores, R_{AAO}, whereas molecules passing through porous graphene experience the resistance due to selective pores, R_s, in series with the support pore. Membrane permeance is proportional to the inverse of the equivalent resistance. The present membrane design isolates defects, such that each defect affects only the support pore over which the defect is located and reduces the graphene coverage, γ (Figure 1a, inset). The effect of defects is therefore included as a small reduction in the graphene coverage, allowing for such a simple resistance network model to be used.

To estimate the selective pore resistance (R_s), a log-normal pore size distribution (Figure 5c) was assumed with mean, μ, and standard deviation, σ. This is often a good model for skewed probability distributions of positive quantities near zero[28] and was found to accurately represent size distributions of pores created in graphene by permanganate etching.[18]. Given this pore size distribution, we construct a simple estimate for the available pore area for gas transport by reducing the pore diameter by the gas molecule kinetic diameter in order to capture steric exclusion to leading order (Figure 5d). The permeance of the nanoporous graphene due to the selective pores is then calculated from the available pore area using the rate of incidence of gas molecules per unit area predicted by the kinetic theory of gases (eq S14). The resistance of graphene due to selective pores is equal to the inverse of the product of this permeance and the support pore area. A more detailed description of this model is presented in Supporting Information Section V.

This model can be used to estimate the permeance of gases of a given kinetic diameter, but requires specification of the graphene coverage (γ), selective pore density (ρ_s), and pore size distribution (μ, σ). These parameters are determined by fitting the model to the measured flow rate data for gases over a range of kinetic diameters (Figure 5e). The model accurately captures the trends in flow rate (Figure 5e) and normalized selectivity (Figure 5f).

Corroboration for the model is provided by the values obtained for the graphene coverage and selective pore density fitting parameters. The fitted coverage of 68% is within the experimental uncertainty in the coverage of 73% as measured independently by gas flow experiments prior to ion bombardment (Table S1). Note also that, if nanometer-scale pores are created by etching, these may have lower resistance to flow than the support pore and effectively act as tears, so that the coverage after plasma exposure is likely lower than that measured before treatment. In addition, clamping/unclamping of the membrane may also contribute to a slightly reduced coverage. The fitted density of selective pores larger than the

DOI: 10.1021/acsnano.7b01231
ACS Nano 2017, 11, 5726−5736

kinetic diameter of helium (2.6×10^{12} cm^{-2}) is in the expected range for the ion bombardment density of 2×10^{13} cm^{-2}.[29]

It is possible to similarly fit a model using the measured pore size distribution in Figure 3a, rather than a generic log-normal distribution. This was done using the graphene coverage (γ) and selective pore density (ρ_s) as fitting parameters and is also shown in Figure 5e,f. However, since the total graphene area that could reasonably be imaged at sufficiently high magnification to determine pore size was limited, there is significant uncertainty in the measured pore size distribution. From Figure 3a, we see that only seven helium permeable pores were observed in the 6400 nm^2 area that was imaged. Nevertheless, the model with this distribution captures the general trends in normalized flow rate (Figure 5e) and normalized selectivity (Figure 5f) with kinetic diameter. Furthermore, the fitted parameters are again in reasonable agreement with measurement, giving 70% coverage as compared to the measured value of 73% and a pore density of 2.5×10^{11} cm^{-2} as compared to 1.1×10^{11} cm^{-2} estimated from STEM images (Figure 3). However, the fitted pore density is lower than that in the log-normal case because the helium-permeable pores are larger on average in the measured pore size distribution (Figure 3a).

This modeling provides a quantitative explanation for the experimentally observed saturation in the measured normalized selectivity as the kinetic diameter increases (Figure 5f). For $\gamma = 1$, that is, complete coverage, the model predicts that the normalized selectivity relative to helium continues to increase with kinetic diameter. However, for $\gamma < 1$, leakage flow dominates for larger molecules. This can be explained by noting that for large gas molecules, this leakage is significantly higher than the associated permeance due to selective pores in graphene, *i.e.*, $\frac{R_{AAO}}{1-\gamma} \ll \frac{R_s + R_{AAO}}{\gamma}$ since the resistance due to the selective pores, R_s, is large for the larger gas molecules (see Figure 5b). In other words, the normalized selectivity exhibits an upper bound because leakage through support pores that are not covered by graphene (a fraction, $1 - \gamma$, of the pores) exceeds the contribution of regions covered by graphene. The experimentally measured saturation of normalized selectivity for larger molecule kinetic diameters is therefore a further illustration of the significant effect that leakage has on the performance of graphene membranes.

Graphene Membrane Performance. The measured overall membrane performance is plotted in Figure 6 for a selection of gas pairs. Conventional polymeric membranes are typically compared on permeability–selectivity plots.[1,5] These membranes operate by a solution-diffusion mechanism, and their permeance scales inversely with thickness. Permeability (permeance multiplied by thickness) is then an intrinsic property of the membrane material and can be used for comparison. However, the thickness of single-layer graphene membranes cannot be changed; stacking multiple layers of graphene changes the physics of gas transport through the membrane. Therefore, permeance, not permeability, is the intrinsic material property of graphene membranes. For this reason, Figure 6 presents graphene membrane performance on permeance–selectivity plots. For comparison to the Robeson limit for polymer membranes, an active layer thickness of 100 nm was assumed, which is typically the thinnest possible in such membranes.[3]

The gas permeances measured on the nanoporous graphene membranes on AAO supports also provide useful information about the properties of nanoporous graphene in the absence of tears and the support substrate. By measuring the flow rate through the membrane prior to ion bombardment and using the equivalent resistance network in Figure 5b, we can estimate the fraction of AAO pores covered with graphene as, $\gamma = 1 - J_A/J_A^0$ (Table S1), where J_A^0 is the measured gas A flow rate through the AAO support prior to graphene transfer and J_A is the measured gas A flow rate through the membrane after graphene transfer. The gas used to estimate this coverage was SF_6. Assuming that flow through AAO pores that are not covered by graphene is unchanged by ion bombardment and plasma etching (based on control experiments in Figure S4), and without modeling the selective pore resistance, we can estimate the permeance and selectivity of just the nanoporous graphene (Figure 6, details in Supporting Information Section VI):

$$s_{A/B} = \frac{J_A^0 \left[\left(\frac{J'_B}{J_B} - 1\right)\left(\frac{1-\gamma}{\gamma}\right)\right]^{-1} - 1}{J_B^0 \left[\left(\frac{J'_A}{J_A} - 1\right)\left(\frac{1-\gamma}{\gamma}\right)\right]^{-1} - 1} \quad (1)$$

Here, $s_{A/B}$ is the extracted nanoporous graphene selectivity of gas A over gas B and J'_A is the measured gas A flow rate through the membrane after graphene transfer and selective pore creation. The *extracted* nanoporous graphene permeance and selectivity values represent the measured upper bound on membrane performance achievable with the nanoporous graphene created in this study, if tears could somehow be completely eliminated and the support membrane had 100% porosity with no resistance to gas flow. However, in the case of tears/defects resulting in a graphene coverage $\gamma < 1$, the overall membrane selectivity ($S_{A/B}$) is limited by graphene coverage to a maximum achievable value of

$$S_{A/B} = \frac{J_A^0}{J_B^0}\frac{1}{1-\gamma} \quad (2)$$

where the selective pore resistance is zero for gas A and infinite for gas B.

For He/SF_6 separation with the coverage of 73% obtained here, the estimated nanoporous graphene selectivity is 22.4, as compared to 8.4 achieved for the overall membrane. Compared to the measurements of Celebi *et al.*[11] for H_2/CO_2 on a dense array of 7.6 nm pores (selectivity ~3.4), our results exhibit significantly lower permeance but superior selectivity (~7), as expected, since the porosity of our membrane is lower, but the pores are sufficiently small to achieve molecular sieving. Compared to the measurements of Koenig *et al.*[20] for H_2/CH_4 through a single nanopore in a micron-scale area of graphene, our results exhibit significantly lower selectivity (due to the finite width of our pore size distribution, see Figure 3a) but significantly higher permeance due to the higher pore density. Graphene oxide membranes, which take advantage of layering to reduce leakage, have been prepared with significantly higher H_2/CO_2 selectivity (~3400)[30] than estimated for nanoporous graphene here (Figure 6c). However, this selectivity comes at the cost of permeance, which is ~100-fold lower.

It is instructive to compare the extracted graphene performance to the Robeson limit, *i.e.*, the upper bound on polymer separation membrane permeability-selectivity performance for a particular gas pair.[5] Assuming that the polymer

DOI: 10.1021/acsnano.7b01231
ACS Nano 2017, 11, 5726–5736

membranes have a selective layer thickness of 100 nm, the H_2/CH_4 performance is slightly below the Robeson limit, competitive with polymer membranes with selectivities just above the Knudsen value. The H_2/CO_2 performance exceeds this limit.

The estimated nanoporous graphene performance also makes it possible to directly compare our measurements to the estimated separation performance of nanoporous graphene with pore distributions created by other methods (for example, ion bombardment followed by either oxygen plasma or permanganate etching, although permanganate etching is incompatible with the AAO support membrane). Figure 6 shows the estimated performance for pores created by a variety of methods, computed as described in Supporting Information Section VII. The predicted selectivities for these pores compare well with our measured selectivities except for He/SF_6; however, the measured permeance is approximately an order of magnitude below the predicted values. Contamination covering the graphene pores during measurement could contribute to this lower permeance, although we have seen relatively little time-dependent decrease of flux in our measurements, indicating the absence of severe fouling with time. The low extracted He/SF_6 selectivity may be due to slight damage to the membrane during clamping/unclamping; even a small decrease in graphene coverage will significantly reduce the extracted selectivity since it is based on the graphene coverage measured prior to ion bombardment. On the other hand, the simple transport model used in estimating gas permeance from the measured pore size distribution could introduce significant error into those estimates.

CONCLUSIONS

In this work, we have demonstrated selective gas transport using nanoporous graphene membranes at significantly larger scales than previous work. Whereas Koenig *et al.*[20] measured graphene with ~1 pore and Celebi *et al.*[11] measured graphene with $\sim 10^6$ individually machined pores, our membranes feature $\sim 10^{11}$ permeable pores. Previous studies have measured single or few subnanometer selective pores in microscale areas of defect-free graphene[20] or arrays of relatively large (~8 nm) pores[11] where the permeance of selective pores is much higher than that through defects. However, large area membranes with subnanometer selective pores are much more sensitive to leakage through defects, necessitating scalable defect mitigation strategies, a number of which have been proposed, analyzed, and discussed in this paper.

This study focused on two major issues associated with graphene membrane scalability: the design and fabrication of defect-tolerant membranes and methods to produce gas-selective pores in graphene with high density over large areas. Based on multiscale modeling of gas transport, the support membrane structure was chosen to isolate small defects and limit leakage through large defects. Ion bombardment followed by oxygen plasma etching was shown to produce a high density of pores with subnanometer size, suitable for gas separation. This led to measurable molecular-sieving-based selective gas transport through centimeter-scale areas of graphene.

The extracted graphene gas separation performance for H_2/CH_4 was competitive with the Robeson limit and that for H_2/CO_2 exceeded the Robeson limit. However, it is important to note that this estimate relates only to nanoporous graphene. The overall membrane has tears and a support with limited porosity, which reduces permeance and selectivity. Although gas selectivity was achieved with a large number of pores over relatively large areas, the measured overall membrane selectivity and permeance were lower than have been predicted possible with graphene,[7−9,21] highlighting the opportunity for further advancements. Despite predictions of graphene membrane gas selectivities far exceeding those of conventional membranes,[7−9,21] even a low level of defects in graphene will limit their use to separations with modest purity requirements. Due to similar considerations, conventional membranes are often not the method of choice for high-purity separations.[1−3,31] Further work is therefore required in pore creation as well as leakage mitigation or defect sealing to improve the selectivity of nanoporous graphene.

Advances in membrane fabrication are required to bring the performance of graphene membranes closer to their potential. More robust support structures, such as polymeric membranes with a resistance-matched layer that is thinner than the average spacing between defects, are necessary for practical applications. Improvements in graphene quality and defect sealing can raise overall membrane performance toward the estimated nanoporous graphene performance measured in this study. Increasing selectivity beyond this value will require methods for creating narrower selective pore size distributions or use of other means such as chemical functionalization of the graphene pores. The estimated permeance of nanoporous graphene is orders of magnitude higher than most membranes, but higher densities of pores could further increase the permeance. The membrane permeance model developed in this study can be used to quantify the required improvements and guide future developments (Supporting Information Section IX and Figure S7). Although significant challenges remain in developing high-performance graphene membranes on the scale necessary for practical separations, graphene membranes could significantly benefit industrial separation processes if their full potential is realized.

METHODS

Graphene Transfer to AAO Membrane Supports. AAO membranes (InRedox, 10 mm disks, 20 nm pore diameter, 50 μm thickness) were hand polished on an alumina surface (Spyderco, ultrafine) once and on a 100 nm diamond lapping film (Ted Pella) twice. Each polishing step consisted of 90 s of polishing, followed by a submersion in 10% sulfuric acid for 30 s, to dissolve removed alumina dust, followed by rinsing in water. Acid exposure times were kept short so as not to damage the AAO structure. CVD graphene (Graphenea, Figure S9) on copper was pre-etched for 2 min by floating on ammonium persulfate (Transene, APS-100) and then rinsing in water to wash away curled up graphene from the back side of the copper foil. The remaining copper was then etched away by floating on ammonium persulfate, leaving graphene floating on the etchant surface. The polished AAO was then gently pressed against the graphene using a vacuum TEM grid holder (Ted Pella), scooped out with a glass slide onto water to rinse, and air-dried. A more detailed description of the graphene transfer process is provided in Supporting Information Section II. The membrane fabrication yield, starting from an unpolished AAO membrane and finishing with graphene supported on a polished AAO membrane, was approximately 15%. The common failure mechanisms for this transfer process were cracking of the brittle AAO supports during polishing, graphene tearing and curling up on the AAO membrane surface upon contact, and backside wetting of the AAO membrane by the copper etchant causing it to tear through the floating graphene as it sinks.

Selective Pore Creation. Selective pores were introduced in graphene on AAO supports by first bombarding the sample with gallium ions in an FEI Helios Nanolab DualBeam 600 at the MIT Center for Materials Science and Engineering. Bombardment was

DOI: 10.1021/acsnano.7b01231
ACS Nano 2017, 11, 5726−5736

performed at densities of 2−6 × 10^{13} ions/cm^2, an accelerating voltage of 8 kV, current of 19 nA, and an angle of 52°. The samples were then exposed to oxygen plasma (Harrick Plasma Expanded Plasma Cleaner PDC-001, maximum 30 W power, low-power setting, 600 mTorr O_2) for the desired time increment. Prior to each oxygen plasma exposure, the chamber was cleaned for 3 min on the high-power setting at 600 mTorr O_2.

Gas Flow Measurements. Gas flow rate measurements were performed using the apparatus shown in Figure S3. The membrane was mounted in an AAO holder (InRedox) between an upstream pressure line and downstream reservoir. Both sides of the membrane were pumped to vacuum before supplying a single gas species at 1 atm pressure upstream. The slope of the pressure *versus* time history measured with a pressure transducer (Omega Engineering) in the downstream reservoir was used with the ideal gas law to calculate the gas flow rate. Permeance measurements were performed at an ambient temperature of 20 °C. Further details are provided in the Supporting Information.

SEM Imaging. SEM imaging was performed with an FEI Helios Nanolab DualBeam 600 at the MIT Center for Materials Science and Engineering. Imaging was performed at 2 kV, 86 pA, in immersion mode, employing an Everhart-Thornley detector. AAO surface roughness was visualized before and after polishing by first sputter coating the samples with 2 nm of platinum/palladium (80%/20%) and then imaging at an angle of 52°. Graphene on the AAO was imaged at an angle of 0° using carbon tape to make a conductive path from the graphene to the SEM stub.

STEM Imaging. CVD grown graphene (Graphenea) was transferred onto gold TEM grids (Ted Pella) using ammonium persulfate etchant by the procedure described in ref 13. Graphene on the TEM grid was then bombarded with gallium ions at 5 × 10^{12} ions/cm^2, 52° incidence, and 1 kV accelerating voltage, and oxygen plasma etched for 30 s. Immediately before imaging, the samples were heated to 160 °C at 10^{-5} Torr for 10 h and then allowed to cool under vacuum. Aberration-corrected STEM imaging was performed on a Nion UltraSTEM 100 (ref 32) at Oak Ridge National Laboratory's Center for Nanophase Materials Sciences. Imaging was performed at 60 kV using a semiconvergence angle of 30 mrad and a medium angle annular dark-field detector with ∼54−200 mrad half angle range.

ASSOCIATED CONTENT

Supporting Information

The Supporting Information is available free of charge on the ACS Publications website at DOI: 10.1021/acsnano.7b01231.

Gas transport model, additional methods, analysis, and control experiments, and supplementary discussion (PDF)

AUTHOR INFORMATION

Corresponding Authors

*E-mail: ngh@mit.edu.
*E-mail: karnik@mit.edu.

ORCID

Rohit Karnik: 0000-0003-0588-9286

Notes

The authors declare the following competing financial interest(s): R.K. discloses financial interest in a company aimed at commercializing graphene membranes.

ACKNOWLEDGMENTS

This research was funded in part by an MIT Energy Initiative seed grant and in part by the U.S. Department of Energy Office of Basic Energy Sciences award number DE-SC0008059. M.S.H.B. acknowledges support from the Natural Sciences and Engineering Research Council of Canada (NSERC) postgraduate scholarships program. The authors acknowledge helpful discussions with Sean O'Hern, Jongho Lee, Suman Bose, Tarun Jain, Luda Wang, and William Koros. We also thank Krithika Ramchander for assisting with permeance measurement calibration. STEM imaging was performed as a part of a user proposal at Oak Ridge National Laboratory, Center for Nanophase Materials Sciences (CNMS), supported by the Scientific User Facilities Division, Office of Basic Energy Sciences, U.S. Department of Energy (JCI). This work made use of facilities at the Center for Nanoscale Systems (CNS) at Harvard University, a member of the National Nanotechnology Infrastructure Network, supported by the National Science Foundation under NSF award no. ECS-0335765, and the MRSEC Shared Experimental Facilities at MIT, supported by the National Science Foundation under award number DMR-1419807.

REFERENCES

(1) Baker, R. W. Future Directions of Membrane Gas Separation Technology. *Ind. Eng. Chem. Res.* **2002**, *41*, 1393−1411.
(2) Baker, R. W.; Low, B. T. Gas Separation Membrane Materials: A Perspective. *Macromolecules* **2014**, *47*, 6999−7013.
(3) Baker, R. W. *Membrane Technology and Applications*; John Wiley & Sons, Ltd: Chichester, UK, 2004.
(4) Sholl, D. S.; Lively, R. P. Seven Chemical Separations to Change the World. *Nature* **2016**, *532*, 435−437.
(5) Robeson, L. M. The Upper Bound Revisited. *J. Membr. Sci.* **2008**, *320*, 390−400.
(6) Bunch, J. S.; Verbridge, S. S.; Alden, J. S.; van der Zande, A. M.; Parpia, J. M.; Craighead, H. G.; McEuen, P. L. Impermeable Atomic Membranes from Graphene Sheets. *Nano Lett.* **2008**, *8*, 2458−2462.
(7) Hauser, A. W.; Schwerdtfeger, P. Methane-Selective Nanoporous Graphene Membranes for Gas Purification. *Phys. Chem. Chem. Phys.* **2012**, *14*, 13292.
(8) Liu, H.; Dai, S.; Jiang, D. Permeance of H2 through Porous Graphene from Molecular Dynamics. *Solid State Commun.* **2013**, *175*−*176*, 101−105.
(9) Schrier, J. Helium Separation Using Porous Graphene Membranes. *J. Phys. Chem. Lett.* **2010**, *1*, 2284−2287.
(10) Koenig, S. P.; Boddeti, N. G.; Dunn, M. L.; Bunch, J. S. Ultrastrong Adhesion of Graphene Membranes. *Nat. Nanotechnol.* **2011**, *6*, 543−546.
(11) Celebi, K.; Buchheim, J.; Wyss, R. M.; Droudian, A.; Gasser, P.; Shorubalko, I.; Kye, J.-I.; Lee, C.; Park, H. G. Ultimate Permeation across Atomically Thin Porous Graphene. *Science* **2014**, *344*, 289−292.
(12) Breck, D. W. *Zeolite Molecular Sieves: Structure, Chemistry, and Use*; John Wiley and Sons: New York, 1974.
(13) O'Hern, S. C.; Stewart, C. A.; Boutilier, M. S. H.; Idrobo, J.-C.; Bhaviripudi, S.; Das, S. K.; Kong, J.; Laoui, T.; Atieh, M.; Karnik, R. Selective Molecular Transport through Intrinsic Defects in a Single Layer of CVD Graphene. *ACS Nano* **2012**, *6*, 10130−10138.
(14) Boutilier, M. S. H.; Sun, C.; O'Hern, S. C.; Au, H.; Hadjiconstantinou, N. G.; Karnik, R. Implications of Permeation through Intrinsic Defects in Graphene on the Design of Defect-Tolerant Membranes for Gas Separation. *ACS Nano* **2014**, *8*, 841−849.
(15) Surwade, S. P.; Smirnov, S. N.; Vlassiouk, I. V.; Unocic, R. R.; Veith, G. M.; Dai, S.; Mahurin, S. M. Water Desalination Using Nanoporous Single-Layer Graphene. *Nat. Nanotechnol.* **2015**, *10*, 459−464.
(16) Koh, D.-Y.; Lively, R. P. Nanoporous Graphene: Membranes at the Limit. *Nat. Nanotechnol.* **2015**, *10*, 385−386.
(17) Kim, H. W.; Yoon, H. W.; Yoon, S.-M.; Yoo, B. M.; Ahn, B. K.; Cho, Y. H.; Shin, H. J.; Yang, H.; Paik, U.; Kwon, S.; Choi, J.-Y.; Park, H. B. Selective Gas Transport Through Few-Layered Graphene and Graphene Oxide Membranes. *Science* **2013**, *342*, 91−95.

DOI: 10.1021/acsnano.7b01231
ACS Nano 2017, 11, 5726−5736

(18) O'Hern, S. C.; Boutilier, M. S. H.; Idrobo, J.-C.; Song, Y.; Kong, J.; Laoui, T.; Atieh, M.; Karnik, R. Selective Ionic Transport through Tunable Subnanometer Pores in Single-Layer Graphene Membranes. *Nano Lett.* **2014**, *14*, 1234−1241.
(19) O'Hern, S. C.; Jang, D.; Bose, S.; Idrobo, J.-C.; Song, Y.; Laoui, T.; Kong, J.; Karnik, R. Nanofiltration across Defect-Sealed Nanoporous Monolayer Graphene. *Nano Lett.* **2015**, *15*, 3254−3260.
(20) Koenig, S. P.; Wang, L.; Pellegrino, J.; Bunch, J. S. Selective Molecular Sieving through Porous Graphene. *Nat. Nanotechnol.* **2012**, *7*, 728−732.
(21) Au, H. Molecular Dynamics Simulation of Nanoporous Graphene for Selective Gas Separation. MS Thesis, Massachusetts Institute of Technology, 2012.
(22) Russo, C. J.; Golovchenko, J. A. Atom-by-Atom Nucleation and Growth of Graphene Nanopores. *Proc. Natl. Acad. Sci. U. S. A.* **2012**, *109*, 5953−5957.
(23) Schrier, J. Fluorinated and Nanoporous Graphene Materials as Sorbents for Gas Separations. *ACS Appl. Mater. Interfaces* **2011**, *3*, 4451−4458.
(24) Schrier, J. Carbon Dioxide Separation with a Two-Dimensional Polymer Membrane. *ACS Appl. Mater. Interfaces* **2012**, *4*, 3745−3752.
(25) Shan, M.; Xue, Q.; Jing, N.; Ling, C.; Zhang, T.; Yan, Z.; Zheng, J. Influence of Chemical Functionalization on the CO2/N2 Separation Performance of Porous Graphene Membranes. *Nanoscale* **2012**, *4*, 5477.
(26) Sun, C.; Boutilier, M. S. H.; Au, H.; Poesio, P.; Bai, B.; Karnik, R.; Hadjiconstantinou, N. G. Mechanisms of Molecular Permeation through Nanoporous Graphene Membranes. *Langmuir* **2014**, *30*, 675−682.
(27) Wen, B.; Sun, C.; Bai, B. Inhibition Effect of a Non-Permeating Component on Gas Permeability of Nanoporous Graphene Membranes. *Phys. Chem. Chem. Phys.* **2015**, *17*, 23619−23626.
(28) Limpert, E.; Stahel, W. A.; Abbt, M. Log-Normal Distributions across the Sciences: Keys and Clues. *BioScience* **2001**, *51*, 341.
(29) Lehtinen, O.; Kotakoski, J.; Krasheninnikov, A. V.; Keinonen, J. Cutting and Controlled Modification of Graphene with Ion Beams. *Nanotechnology* **2011**, *22*, 175306.
(30) Li, H.; Song, Z.; Zhang, X.; Huang, Y.; Li, S.; Mao, Y.; Ploehn, H. J.; Bao, Y.; Yu, M. Ultrathin, Molecular-Sieving Graphene Oxide Membranes for Selective Hydrogen Separation. *Science* **2013**, *342*, 95−98.
(31) Baker, R. W.; Lokhandwala, K. Natural Gas Processing with Membranes: An Overview. *Ind. Eng. Chem. Res.* **2008**, *47*, 2109−2121.
(32) Krivanek, O. L.; Corbin, G. J.; Dellby, N.; Elston, B. F.; Keyse, R. J.; Murfitt, M. F.; Own, C. S.; Szilagyi, Z. S.; Woodruff, J. W. An Electron Microscope for the Aberration-Corrected Era. *Ultramicroscopy* **2008**, *108*, 179−195.

DOI: 10.1021/acsnano.7b01231
ACS Nano 2017, 11, 5726−5736